Fifteenth Quarterly Progress Report

February 1, 2010 to April 30, 2010
Contract No. HHS-N-260-2006-00005-C
Neurophysiological Studies of Electrical Stimulation for the Vestibular Nerve
Submitted by:

James O. Phillips, Ph.D.[1,3,4]
Steven Bierer, Ph.D. [1,3,4]
Albert F. Fuchs, Ph.D. [2,3,4]
Chris R.S. Kaneko, Ph.D. [2,3]
Leo Ling, Ph.D. [2,3]
Shawn Newlands, M.D., Ph.D. [5]
Kaibao Nie, Ph.D. [1,4]
Jay T. Rubinstein, M.D., Ph.D. [1,4,6]

[1] Department of Otolaryngology-HNS, University of Washington, Seattle, Washington
[2] Department of Physiology and Biophysics, University of Washington, Seattle, Washington
[3] Washington National Primate Research Center, University of Washington, Seattle, Washington
[4] Virginia Merrill Bloedel Hearing Research Center, University of Washington, Seattle, Washington
[5] Department of Otolaryngology, University of Rochester, Rochester, New York
[6] Department of Bioengineering, University of Washington, Seattle, Washington

Reporting Period: February 1, 2010 to April 30, 2010

Challenges: Our two main challenges for this quarter have been software development and surgical issues. We have a continuing challenge with multiple single unit recording electrode fabrication and design.

1. Our development of software for the lower level SDK programming environment continues to progress slowly, despite the fact that this was given a high priority in the last quarterly progress report and we have spent a significant amount of time on the SDK code development. Although we have enjoyed considerable success in implementing real time frequency modulated stimulus generation using the audio input and the SDK programming environment, which is shown below, we still have not been able to drive the device with an auxiliary input as opposed to the microphone input, which is an essential step in full implementation of this approach as a solution for real time processing in vivo. Also, we have not made progress on our objective of evaluating the apparent differences in current level between real time processing on the bench top and real time processing in vivo. This is partly due to the ongoing changes that are taking place in the lower level software. Until we have a stable system that can be driven with the auxiliary input in the SDK environment, we will be unable to evaluate the differences in performance between the NIC 2 and the SDK implementations of our software in vivo, which is critical to the success of this subproject.

Our response to this challenge has been to ask Dr. Nie to continue devote his full contract effort of 20% FTE to this subproject in Quarter 16, with the assistance of Dr. Rubinstein as outlined in QPR 14. In addition, Dr. Nie has been in contact with Cochlear Corporation for their guidance so that he can build new firmware in order to use the auxiliary input port, which is not available in code debugging mode.

2. Our surgical approach continues to produce variable success even with the use of intraoperative vECAP. In Quarter 14, we defined a three-canal implant as an important Quarter 15 surgical objective, to meet the requirement of 3 dimensional directional control of evoked eye movements. This objective is still unmet. As of the writing of this document, we have only been able to successfully implant two canals in any single animal with our minimally invasive approach. Dr. Newlands was able to implant three canals successfully using an aggressive reimplantation procedure and canal plugging, but this procedure only produced a relatively short lived implant with two well functioning canal electrodes. While Dr. Rubinstein is confident that he can implant three canals during human implantation, or using an aggressive surgical approach in monkeys, he does not believe that the less invasive surgical procedure can be successfully performed in three canals in rhesus monkeys given their anatomy, and has therefore not attempted it.

We also continue to have the challenge of consistently producing and maintaining functional electrode implants, which produce robust eye movements, in primates that are highly active shortly after surgery. After discussions with our local animal care committee and the veterinary staff, we modified our surgical approach to place and map

2

our chambers prior to implantation of the prosthesis. The objective was to be able to quickly record units if the implant was functional. This change may have contributed to increased edema in a monkey following our last implant surgery. Also, we thought that we had solved the implant stability and placement issues by securing implants with suture and by using vECAP to verify that the leads were optimally placed. One of our last surgeries failed because although the electrodes were successfully placed, as confirmed by vECAP, they migrated following surgery, as confirmed both by vECAP and by a lack of behavioral responses after one week of recovery from surgery. This surgical failure may have been partly the result of a modification in the strategy for securing the implant, which was designed to mirror the proposed human surgical approach.

Our approach to these challenges is to stay the course, and to try to be as consistent as possible in performing the surgery. We still believe in the approach and the strategy, and we are now performing the surgeries without modification from the successful implant surgeries that we have had in the past. We will, however, not attempt implantation of three canals in a monkey until we enjoy consistent success in implanting the lateral and posterior canals in our monkeys.

3. We have not yet received our multiple single unit recording axial electrode arrays from Lawrence Livermore Laboratories. Dr. Satinderpal Pannu has indicated that he has been working on a prototype multichannel polymer electrode array, but we have not yet received a working device, nor do we have a clear design specification for such an array.

Our response to this challenge is to continue our discussions with Dr. Pannu, and continue recording with other technologies. As is shown below, we have enjoyed modest success in recording from multiple units during stimulation in Quarter 15.

Current Successes:

1. In Quarter 15, Drs. Rubinstein and Phillips submitted a revised IDE, which was subsequently approved by the FDA. We now have permission for a clinical trial of a first in man vestibular prosthesis for the treatment of Meniere's disease developed primarily through this contract. The FDA approval is attached as an addendum to this report.

2. We have presented our results at one international meeting this quarter.

Phillips, J.O., Fuchs, A.F., Ling, L., Kaneko, C.R.S., Bierer, S., Nie, K., Newlands, S., Rubinstein, J. *Activation of vestibular neurons and VOR with a vestibular prosthesis.*, 20th Neural Control of Movement Conference, Naples, FL, 2010.

3. We submitted two additional full abstracts and two preliminary abstracts reporting our findings this quarter.

Phillips, J.O., Fuchs, A.F., Ling, L., Kaneko, C.R.S., Bierer, S., Nie, K., Newlands, S., Rubinstein, J. *Discharge frequency versus recruitment coding for a unilateral vestibular implant.* Barany 2010.

Ling, L., Oxford, T., Bierer, S., Fuchs, A., Nie, K., Rubinstein, J., Kaneko, C., Phillips, J. *Parallel Channels of signal processing in the Vestibular Pathway.* Society for Neuroscience Annual Meeting, San Diego, CA 2010

Jay Rubinstein (presenting author, Workshop Preliminary Abstract) Minimally *Invasive Vestibular Implant: 1. Design, surgical implantation and preservation of natural function.* Association for Research in Otolaryngology, Winter 2011 Meeting

Jim Phillips (presenting author, Workshop Preliminary Abstract) *Minimally Invasive Vestibular Implant: 2. Mechanism, behavioral responses and neural recording.* Association for Research in Otolaryngology, Winter 2011 Meeting

4. We have been able to create real time frequency modulated electrical stimulation using the lower level SDK programming environment and the microphone input of the clinical processor. In this quarter, we developed software that can run on the Nucleus SDK (Software Development Kit) research platform for transforming analog chair rotational signals to frequency-modulated (FM) pulse trains in real time. This will offer us the capability of exploring the interaction between natural and electrical stimulation using real-time FM stimuli. To achieve this function, a low-frequency chair rotational signal will be modulated to a high-frequency band with a fixed sinusoidal carrier (e.g. 1000 Hz) and then the modulated signal will be fed into one of the analog input ports on the Nucleus freedom speech processor. The Freedom processor can retrieve the chair signal by envelope extraction and subsequently convert it to frequency-modulated pulse train outputs. As a first step, we created several software modules, including microphone input processing, amplitude modulation extraction and pulse train modulation, to perform real-time processing of analog input signals. The reason we used the microphone as an input source is that the Nucleus Freedom processor is not capable of taking direct analog input in code debugging mode. We plan to switch to using direct analog input by building new stand-alone firmware for the Nucleus Freedom processor.

We have demonstrated the capability of generating real-time FM pulse trains using the SDK platform. Figure 1 shows the analog input signal that we supplied to a Nucleus Freedom microphone (upper panel) and the resulting FM pulse trains (bottom panel) recorded on a digital oscilloscope in real time. The analog signal had a carrier frequency of 1000 Hz and a 2-Hz amplitude modulation (AM) signal at a modulation depth of 50%. As shown in Figure 1, the period of the recorded pulse train followed in phase with the envelope of the input signal. The corresponding pulse train was modulated between 100 pps and 250 pps at 2.0 Hz. The range of frequency modulation and the input sensitivity are fixed in this example, but will be controlled by a mapping function in future experiments.
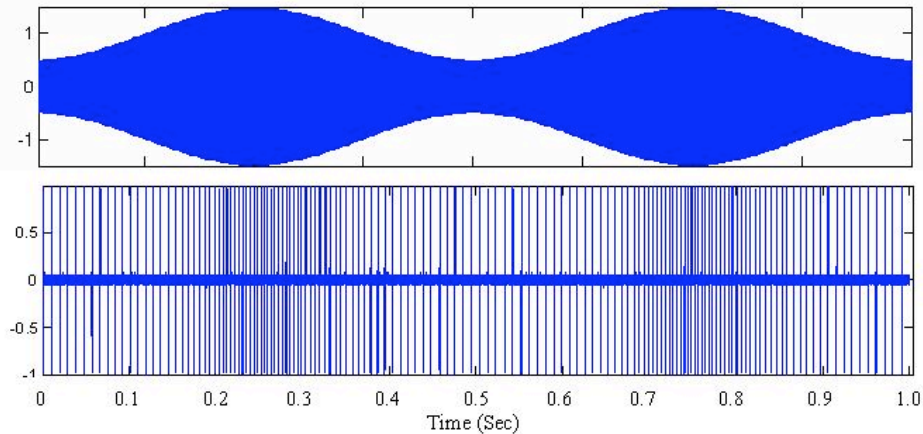
Figure 1.   A 2-Hz AM signal (upper panel) directed to the microphone of a Freedom processor and the real-time FM pulse train output (lower panel) recorded on electrode 22 with an implant-in-a-box simulator while the SDK interface was running in the code-debugging mode.

5. We have improved our capability to isolate electrically driven single-unit spikes within an evoked potential. Our recordings of neural activity in response to electrical stimulation of the vestibular nerve are often characterized by two types of artifact. The initial artifacts, caused by direct volume conduction of each electrical pulse, are brief enough that they do not appreciably affect the detection and classification of single-unit action potentials. At the stimulation frequencies that we typically use, these brief artifacts end before electrically driven single-unit spikes occur. The second type of artifact is an evoked potential, which is likely a summation of local field potentials and low-level spiking activity from multiple neurons in the vicinity of the electrode. Such evoked potentials can obscure otherwise isolated single-unit spikes that are directly driven by the stimulus, because these they occur 1-2 ms after each electrical pulse. In an effort to improve our unit analysis, we have developed a method to effectively subtract every instance of an evoked potential from a recording, revealing the underlying spike waveforms to be detected and classified using standard procedures.

Four segments of recorded activity during electrical stimulation are shown in Figure 2A. The activity was recorded in the vestibular nucleus in response to a 100 µA train of 100 µs biphasic pulses applied at a rate of 10 pps to the lateral canal. Each trace is aligned to one pulse, which occurs at time 0. The first 0.5 ms contains a transient artifact that is nearly identical from one trace to the next. This is followed by the evoked potential, which has a more variable waveform shape. Finally, at 2.5-3.5 ms, a large spike occurs in 3 of the 4 traces. This unit was reliably driven by the 10 pps stimulus. A second lower-amplitude spike waveform was also recorded at this location in the nucleus. It is possible that this second unit was responding to the pulses, with entrained spikes near the 1 ms time mark, but that the spike-like shape of the evoked potential was masking the occurrences.

If the recorded activity following each pulse artifact were to consist of a static "true" evoked potential, with a shape and amplitude that was the same from pulse-to-pulse, plus

a solitary spike waveform with a time of occurrence that varies from pulse-to-pulse as is typical of single units, then it should be possible to subtract the fixed component to recover the spike. The evoked potential traces in Figure 2B are consistent with this hypothesis. Displayed in this panel is a series of 25 evoked waveforms from the same data set as Figure 2A; in this case, time 0 corresponds to 1.2 ms following the preceding electrical pulse (not shown). Note that the positive peaks occur at variable times, and there is substantial jitter in the waveform beginning at t = -0.2 ms. This variability suggests the presence of a single-unit spike riding on top of a static evoked potential.
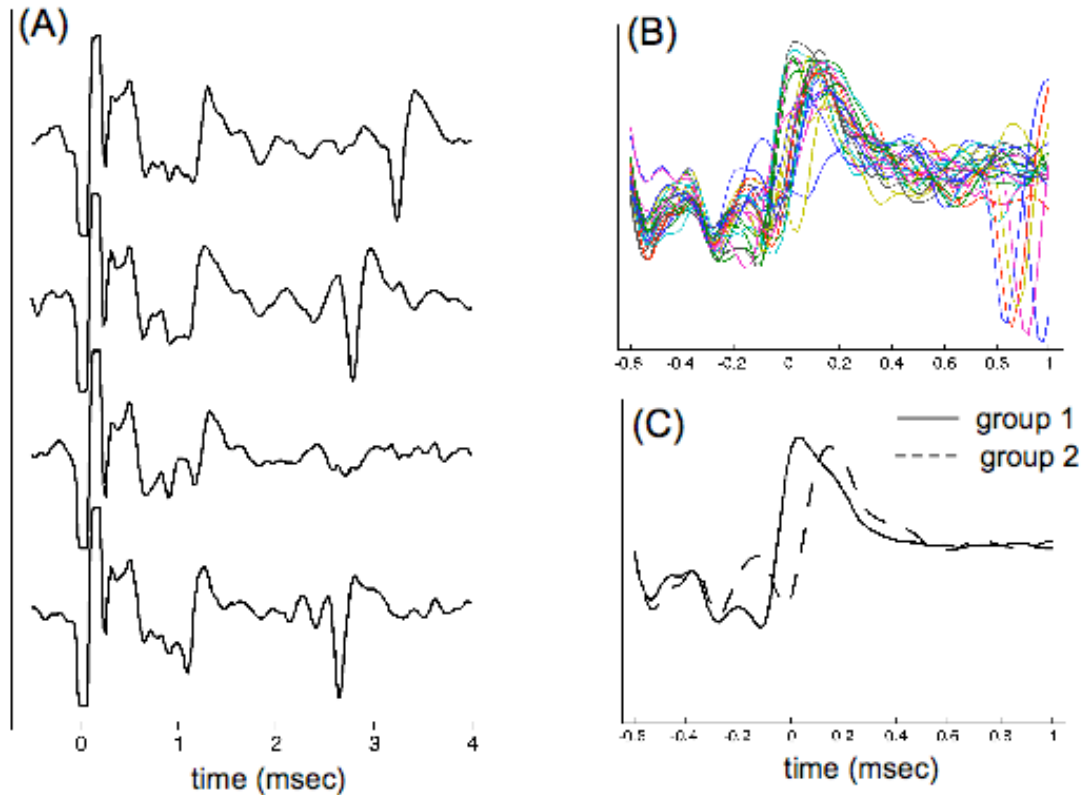

Figure 2. Examples of recorded unit spikes and evoked field potentials during electrical stimulation. A. Units recorded with a field potential. B. 25 superimposed traces from the same data set sampled in part A. C. Evoked potential averages that characterize the two different modes of single unit spike activity.

Recovery of the underlying fixed evoked potential was accomplished in the following manner. In the first step, average waveform shapes of two "modes" of spike firing were obtained, presumably representing an early and late firing latency. This was done by clustering the original waveforms (N=100), in principal component space, into four or more groups using the automatic K-means algorithm. Groups with high standard deviations (indicating spurious isolated spikes) were rejected. An average waveform was calculated for each of the remaining groups, and the two averages that are most dissimilar (assessed by pair-wise cross-correlation) were chosen to represent distinct firing modes of the underlying single-unit spikes. The resulting averaged waveforms for the two

groups representing the evoked potential with the embedded unit occurring at different latencies are shown in Figure 2C.
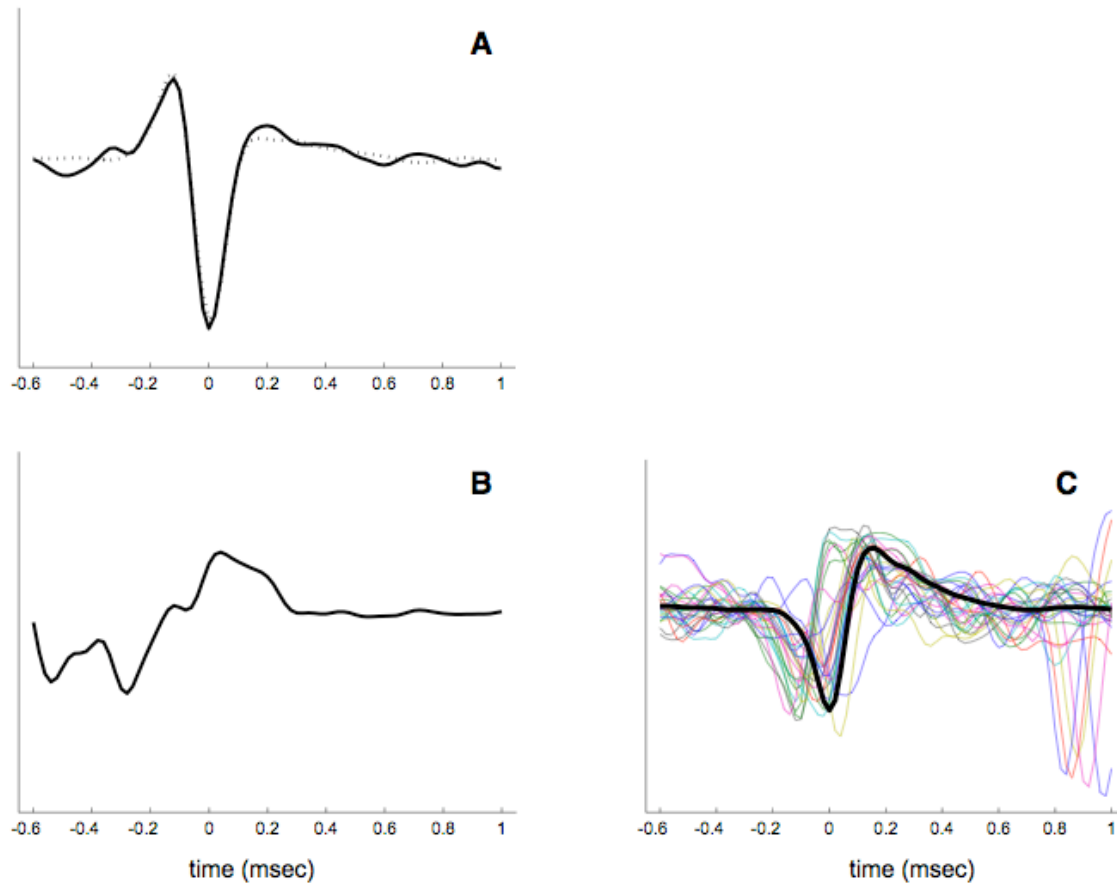

Figure 3. Disambiguation of recorded spikes and evoked field potentials. A. Difference of the two average group waveforms (from Figure 2C) is represented by the solid line; the best fit, based on the template waveform of a well-isolated spike from the same data set, is shown by the dashed line. B. The final "static" evoked potential template, derived by subtracting the spike contributions from the original group averages. C. "Cleaned" version of the waveforms in Figure 2B with the evoked potential template subtracted. The waveforms now resemble the single-unit spike, the template of which is shown by the overlaid thick line.

In the second step, one of the two average waveforms was subtracted from the other. If the static-plus-spike hypothesis is correct, then the static component should cancel and the resulting "difference" waveform should contain primarily contributions from the variably timed spikes. Specifically, the difference waveform should resemble the prototype spike at one latency minus the same prototype spike at a different latency. The prototype spike waveforms, or templates, were formed by averaging spikes that were not corrupted by artifact. These templates were inverted and added together at variable latencies to create a series of "test" templates. A least-squares fitting procedure was then used to determine which spike class and which two latencies best matched the difference waveform. Figure 3A plots the evoked potential difference waveform (solid line) and the

best single-unit template fit (dashed line). In this case, the spike class that gave the best fit was the smaller-amplitude spike.

Finally, the single-unit spike templates at the respective optimal latencies were subtracted from the two evoked potential waveforms. The average of these two waveforms is defined to be the template for the static component of the evoked potential (Figure 3B). In Figure 3C, this template has been subtracted from the original evoked potential waveforms of Figure 2B. The result is a collection of "clean" waveforms that resemble the single-unit spike template (heavy black line), jittered in time from one instance to the next.
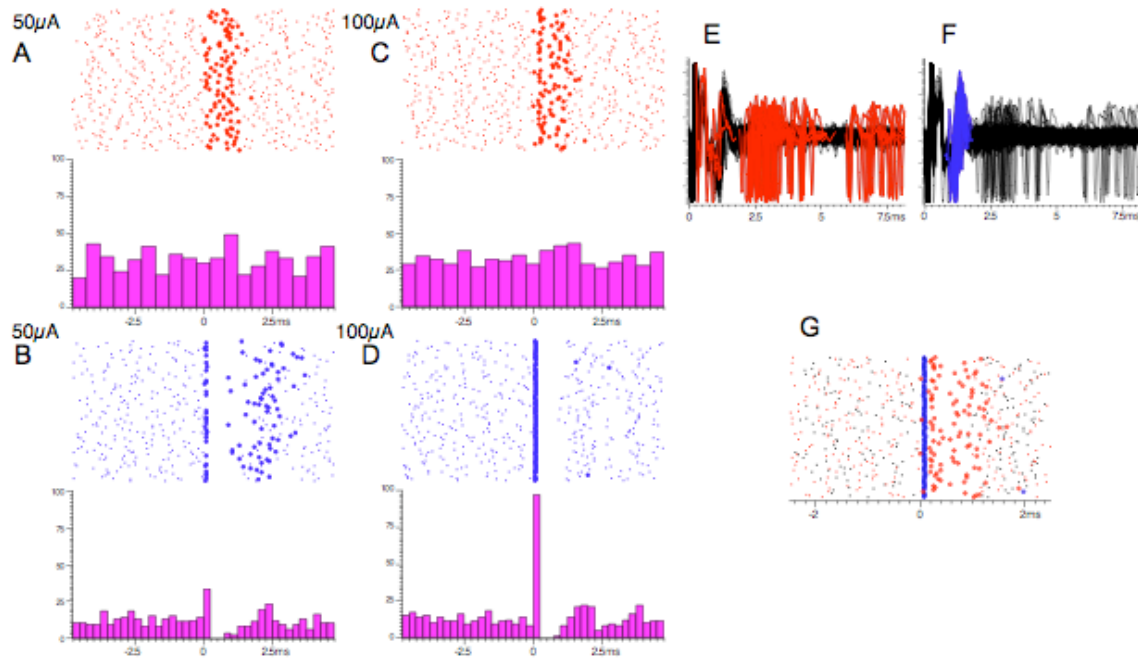

Figure 4. Analysis of the discharge characteristics of the two cleaned units shown in Figures 2 and 3, simultaneously recorded during electrical stimulation at 50 and 100 µA. A,B Unit discharge in response to 50 µA electrical stimulus train at 10 pps. C,D Unit discharge in response to 100 µA electrical stimulus train at 10 pps. E, F Superimposed traces of unit discharge in response to 100 µA electrical stimulus train at 10 pps. G Superimposed histogram for both units at expanded time scale for 100 µA electrical stimulus train at 10 pps.

The cleaned unit traces can then be subjected to further analysis as shown in previous QPRs. Specifically, we can examine the synchrony of discharge at different electrical stimulus current levels for simultaneously recorded neurons. This is shown in Figure 4, which displays histograms for the two cleaned units for constant frequency electrical stimulation at 50 and 100 µA stimulus current levels. Figure 4 displays the first spike following each electrical stimulus as a highlighted colored dot. The longer latency unit is displayed in red, whereas the shorter latency unit is displayed in blue. Figure 4A and 4B show the response of the two units at 50 µA stimulus currents. At this current, the longer latency unit is not driven by the electrical stimulus whereas the shorter latency unit is

driven, with several drop outs, i.e., first post-stimulus spikes occurring at longer latency after the electrical stimulus.   Figures 4C and 4D show the behavior of the units at 100 µA. As this current level, the longer latency unit is driven with some drop outs, and the short latency unit responds at short latency to virtually every electrical stimulus. This is also seen in the superimposed spike waveforms in Figures 4E and 4F, which show the reliable timing of the short latency unit response time locked to the onset of the stimulus. Figure 4G shows a combined histogram for the two units at 100 µA stimulus current at higher temporal resolution, showing the emergence of temporally synchronized discharge in the two units with electrical stimulation at the higher current levels.
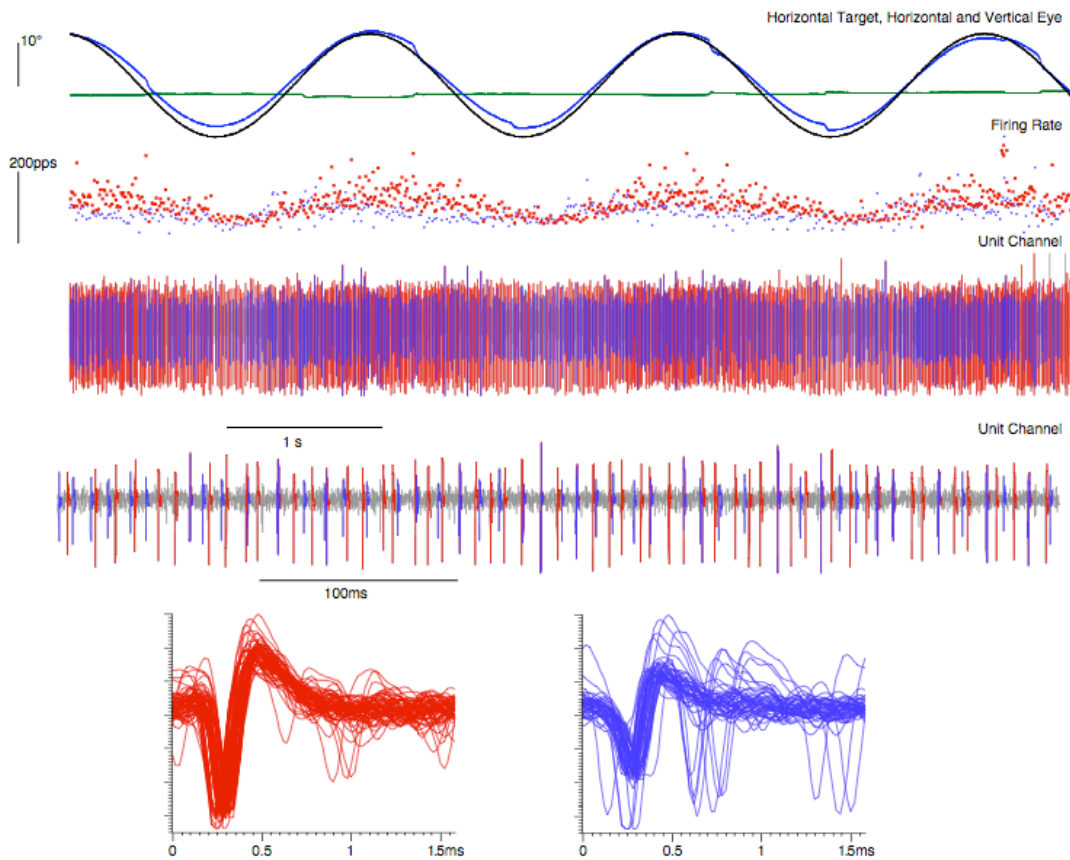

Figure 5. Discharge of the two units displayed in Figures 2-4 during natural rotational stimulation in the plane of the implanted canal. The units are identified by color as in Figure 4. Top traces are horizontal (blue) and vertical eye (red) position and stable in the world target position relative to the head (essentially 180 deg out of phase with chair position, in black). Firing rate. Instantaneous firing rate for each unit is displayed with the colors blue and red identifying each respective unit. Unit Channel (upper).   The recorded spikes of each unit are shown in there respective colors. Unit Channel (lower) The recorded spikes for a single cycle of chair rotation are shown at expanded scale. Insets. Superimposed traces of unit discharge showing the shape of the recorded waveforms.

For comparison, Figure 5 shows the discharge of both units during chair rotation in the dark with an earth stationary fixation spot. Under these conditions, both units show modulated discharge, although the phase of the response differs slightly between units. The units, which are recorded simultaneously, do not show synchrony in their discharge, as is seen in the recorded spike traces expanded at the bottom of Figure 5. Therefore, the emergence of temporally synchronized discharge in the two units as a result of electrical stimulation is related to stimulation current and is not present during natural rotational stimulation of the vestibular end organ.

Utilization of this approach is ongoing in the laboratory and should result in better identification of driven spikes, extraction of multiple units from our existing recorded data, and the analysis of the temporal synchrony of neurons recorded during natural and electrical stimulation.

6. We now have a proposed mechanism for the amplitude (current) modulation of slow phase velocity based on evoked potential recording and accumulated data from single brainstem neurons that are driven during electrical stimulation with the vestibular prosthesis. Our hypothesis is that recruitment is the primary mechanism that controls velocity during constant frequency amplitude modulated electrical stimulation. The critical information for this hypothesis is presented in Figures 6 and 7 below.
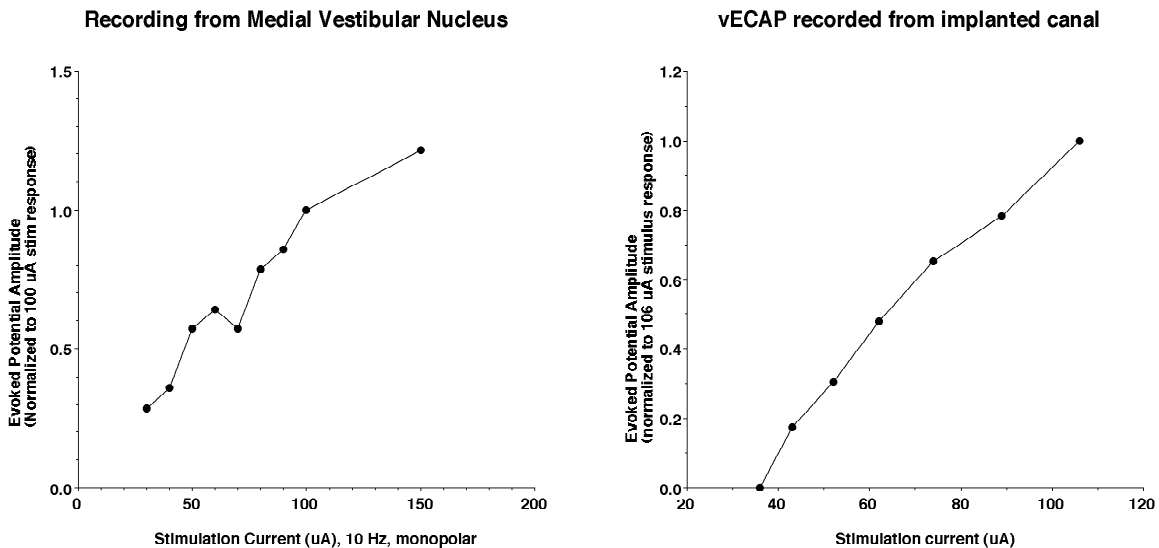

Figure 6. Normalized evoked potential amplitude versus stimulation current recorded in the vestibular nucleus (left panel) and in the vestibular end organ (right panel).

Figure 6 displays the amplitude of the evoked compound action potential recorded both in the vestibular end organ and in the vestibular nucleus. The evoked potential amplitudes are normalized to the potential evoked by 100 μA stimulation in each example. The evoked potentials were recorded in a single animal in response to monopolar electrical stimulation. The brainstem potentials were recorded with a tungsten microelectrode, while the end organ recording was made using neural response telemetry. This example suggests that increasing current produces systematic recruitment of vestibular afferents both at the end organ and at the level of the vestibular nucleus. Such

a signal would only be useful in producing a modulated eye velocity if there was a similar range of current thresholds in brainstem neurons.

Figure 7 displays the distribution and cumulative distribution of current thresholds for responsive vestibular nucleus neurons recorded during electrical stimulation with the vestibular prosthesis. The resulting curve suggests that recruitment across the population of electrically responsive neurons could underlie the modulation of slow phase velocity observed with modulation of stimulus current during constant frequency stimulation. While individual neurons discharge at a relatively constant rate for all currents above threshold, larger numbers of responsive neurons are recruited at higher currents. This mechanism is aphysiologic, in that recruitment does not play an important role in the modulation of vestibular afferents in response to rotational stimuli, but the nervous systems appears to encode increasing numbers of active vestibular neurons as an increasing head velocity signal during electrical stimulation.
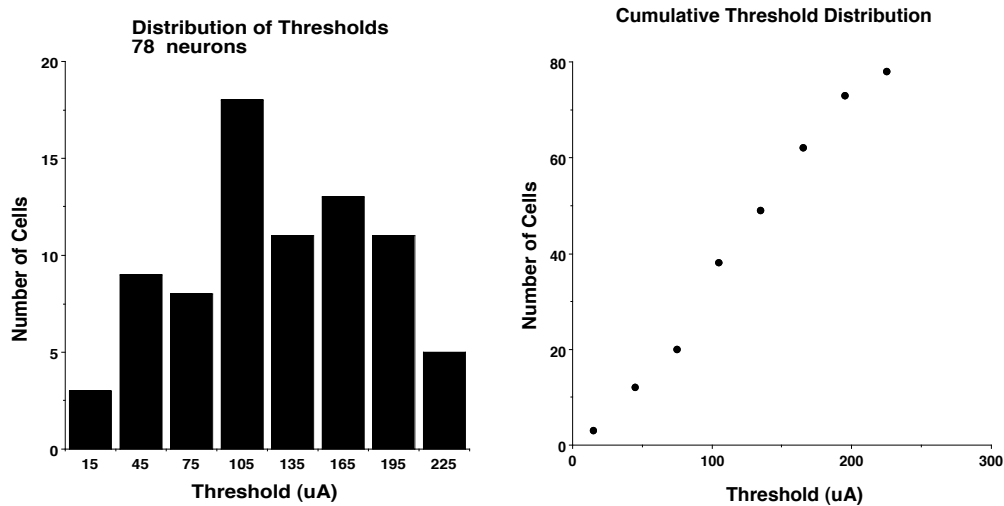

Figure 7. Distribution of current thresholds for electrically responsive neurons recorded in the brainstem during amplitude modulation of a constant frequency vestibular stimulus.

7. We have explored the summation of electrical and natural rotational stimuli in the discharge of single units within the vestibular nucleus and conclude that summation occurs within a single neuron only for very low frequencies of electrical stimulation above current threshold. We are very interested in the neural mechanism underlying summation of natural and electrical stimulus responses to produce a combined response, which is very similar to the linear addition of the electrically elicited slow phase velocity with the rotationally elicited vestibulo-ocular reflex. This is especially interesting given the finding that amplitude modulated electrical stimuli and natural rotational stimuli also appear to add in this way, despite having different apparent mechanisms, one based on recruitment and the other based on frequency modulation. It is possible that single neurons provide some of the integration of these two signals. On the other hand, it is possible that separate neural elements are carrying the two signals.

To evaluate this, we recorded single units during en-bloc rotation of the monkey, and then superimposed a constant frequency electrical stimulus during the ongoing rotation. This paradigm is identical to the paradigm used to elicit a summation of slow phase velocity in behavioral experiments, except that we also asked the animal to suppress its eye movements during the rotation, to eliminate any eye velocity signals that might be carried by the vestibular neuron. In this manner, we could directly compare the rotational vestibular sensitivity of the neuron and the electrical sensitivity of the neuron independently and during combined stimulation. Figure 8 shows the result of one such experiment.
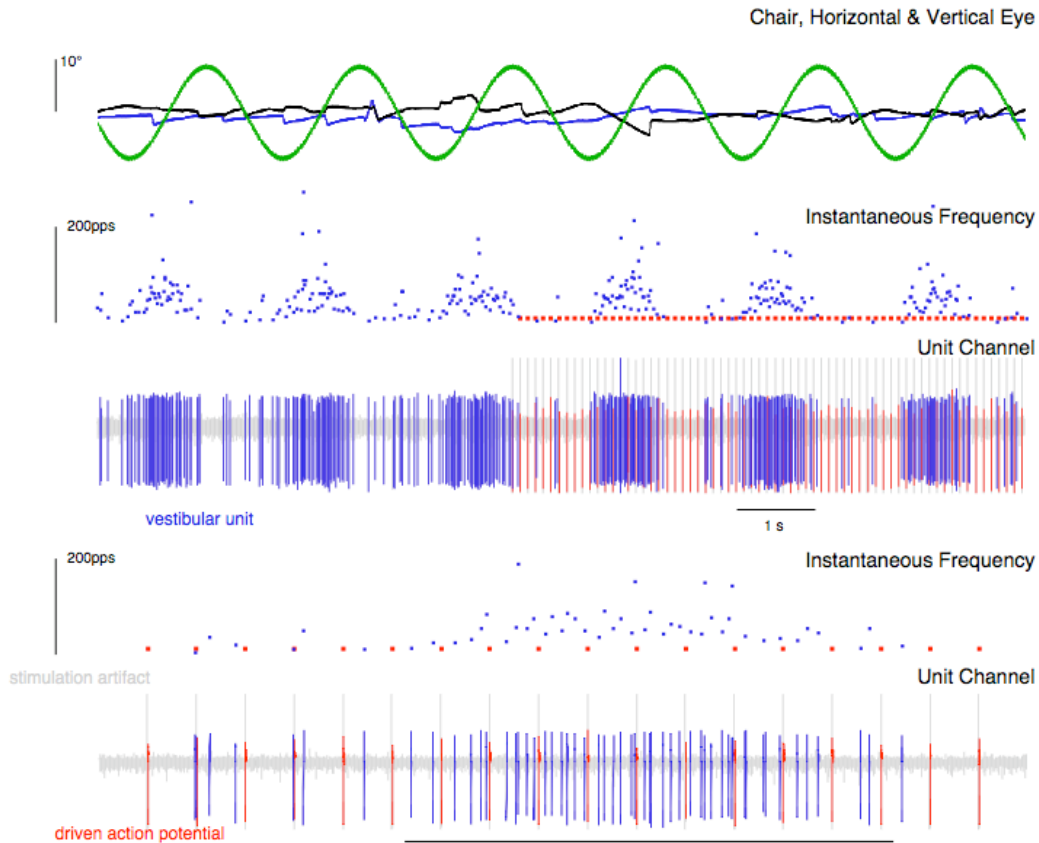

Figure 8. Summation of vestibular and electrical stimulus input in a single vestibular neuron with an electrical stimulation frequency of 10 pps.. Top. Horizontal chair position (green), vertical eye position (blue), horizontal eye position (black), Instantaneous Frequency (upper traces). Unit discharge frequency due to rotation (blue) and time locked to the electrical stimulus (red). Unit Channel (upper traces). Unit spikes due to rotation (blue) and time locked to electrical stimulus (red), and stimulus artifact (grey Instantaneous Frequency (lower traces). Unit discharge frequency due to rotation (blue) and time locked to the electrical stimulus (red) expanded for a single cycle of rotation. Unit Channel (lower traces). Unit spikes due to rotation (blue) and time locked to electrical stimulus (red), and stimulus artifact (grey) expanded for a single cycle of rotation.

In the experiment in Figure 8, the displayed neuron is modulated by horizontal chair rotation during suppression of the VOR without electrical stimulation, and with 10 pps electrical stimulation. As seen in the lower traces, the electrical stimulus simply adds spikes to the modulated activity of the neuron. Therefore, at low stimulation frequency, the neuron performs an integration of both signals and codes for the summed response in its discharge.
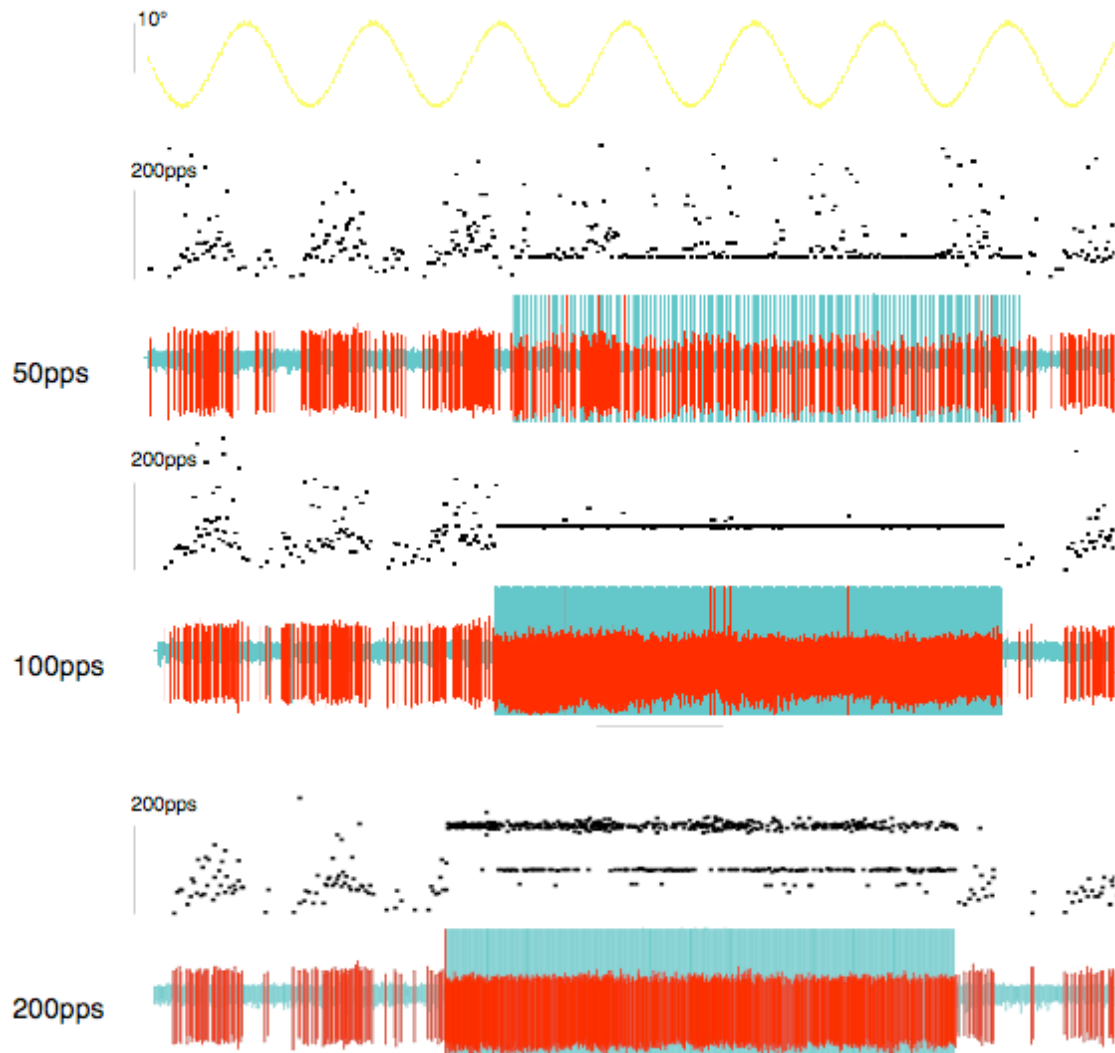

Figure 9. Summation of vestibular and electrical stimulus input in a single vestibular neuron with an electrical stimulation frequency of 50, 100 and 200 pps. (Top, Middle and Lower traces respectively) Traces from top to bottom are chair position (yellow), instantaneous unit discharge frequency (black), unit spikes (red) and stimulus artifact (grey), for each frequency of stimulation.

In the experiment shown in Figure 9, higher frequency electrical stimulation is summed in the same manner with ongoing rotational modulation of the same neuron shown in Figure 8. As the electrical stimulation frequency increases, the modulation of the neuron by rotation becomes less apparent. At the highest frequency, the neuron is driven almost

entirely by the electrical stimulus, although the frequency following of the neuron still appears somewhat modulated by the rotational input (see the drop outs in the instantaneous frequency traces. This complex interaction suggests that summation of the rotational and electrical stimuli does not occur in single driven neurons at higher stimulus frequency. Therefore, summation of rotational and electrical inputs that we have demonstrated behaviorally, must result from activation of independent channels and different neurons by the two stimuli. The precise elements that are responding to each stimulus are not known at this time, but are the subject of ongoing experimentation.

Objectives for Quarter 16.

1. In next quarter, we will continue our software development on the SDK platform. We plan to build firmware to take direct analog inputs instead of feeding the analog signal through the mounted microphone on the Nucleus Freedom processor, and use that input to drive the prosthesis in vivo.

2. We will submit an IRB application for our human clinical study of the safety and efficacy of the vestibular prosthesis for the treatment of Meniere's disease in human subjects. We will begin the study immediately upon receiving approval from the IRB

3. We will continue single unit recording studies with the objective of understanding the precise mechanism that allows for summation of natural and electrical stimuli. We will also pursue recording during natural combined head and eye movements to see if the electrical stimuli are combined with natural stimuli in a physiologically appropriate manner during active head movement.

4. We will present our results in two international meetings, and submit two additional papers.

5. We will continue our ongoing behavioral testing, focusing on recording behavioral responses to parametrically controlled summation of stimulation from two canals.

Addendum to Quarterly Progress Report 15
Conditional FDA Approval of Clinical Study